Applied Thermal Engineering 162 (2019) 114259

Contents lists available at ScienceDirect

Applied Thermal Engineering

journal homepage: www.elsevier.com/locate/apthermeng

An immersed jet array impingement cooling device with distributed returns for direct body liquid cooling of high power electronics

Ruikang Wu, Yiwen Fan, Tao Hong, Hao Zou, Run Hu, Xiaobing Luo*

State Key Laboratory of Coal Combustion, School of Energy and Power Engineering, Huazhong University of Science and Technology, Wuhan 430074, China

HIGHLIGHTS

- A jet array impingement device for direct body liquid cooling is proposed.
- A high power test facility for up to 800 W heat power is established.
- The low temperature rise of 38.7 °C is achieved with heat power of 800 W.
- The maximum effective heat transfer coefficient h = 41,377 W/m^2·K is achieved.
- The combine effect of body cooling and 3D thermal conduction is studied.

ARTICLE INFO

Keywords:
Impingement jet
Direct liquid cooling
High power electronics
TIM
Immersed
Body cooling

ABSTRACT

Heat removal of high-power electronic devices has become the bottleneck that restricts the working performances. For ultrahigh heat flux density, even a thin layer of thermal interface material will dominate the temperature rise along the whole heat dissipation path. The existing liquid cooling only consider the cooling of the top surface of the electronic devices/chips, causing insufficient utilization of the cooling potential. In this paper, an immersed jet array impingement cooling device with distributed returns was designed, fabricated, and tested. In the proposed cooling device, the chip is immersed in the coolant and the coolant is ejected onto all the immersed surface of the electronics through the impinging jets, enabling to provide body cooling for high-power electronics. To prevent the jet interference between adjacent jets, distributed extraction returns were set between the adjacent jets for coolant to exit the impingement domain without flowing past the surrounding jets. The measured average temperature of the high-power chip with input heat power 550 W and flow rate 1000 ml/min is 77.0 °C, where the effective heat flux is 110 W/cm^2, and the inlet coolant temperature is maintained to be 40 °C. The average temperature of the high-power chip under the input heat power of 800 W (160 W/cm^2) is 78.7 °C with the flow rate reaching 2000 ml/min. The effective heat transfer coefficient of 41,377 W/m^2·K in maximum was achieved. The present body cooling is expected to provide high heat removal ability and be used for ultrahigh heat flux density electronics.

1. Introduction

The thermal management of high power electronics, such as the IGBTs, the HEMTs, the LEDs and the high-performance computing chips, has become a critical issue due to the large amount of heat generation, large heat flux and the decreasing feature size [1–7]. Higher temperature causes poorer performance and efficiency [8,9], larger failure rate [10,11] and limits the design power of electronic devices. Active liquid cooling, which includes the microchannel liquid cooling [12], jet impingement liquid cooling [13–15] and spray cooling [16,17], has been validated to be a promising thermal management technique to maintain the temperature of high power electronics with heat flux up to 1 kW/cm^2 within a reasonable range.

Most microchannel cooling techniques are indirect liquid cooling [18–20]. The microchannel heat sink is attached to the electronic device by the TIM. The fluid flows inside the heat sink and never touches the electronic device directly. Therefore, there should be at least a layer of heat sink wall and a layer of TIM lie between the coolant and the electronic device, resulting in large conductive thermal resistance at high heat flux. The thermal conductivity of the commercial TIM is usually less than 5 W/m·K. The TIM has been stated to be even the main bottleneck to reduce the thermal resistance between the coolant and the

* Corresponding author.
E-mail address: luoxb@hust.edu.cn (X. Luo).

https://doi.org/10.1016/j.applthermaleng.2019.114259
Received 5 November 2018; Received in revised form 5 June 2019; Accepted 13 August 2019
Available online 14 August 2019
1359-4311/

high power electronics [21] and it becomes the dominating obstacle in improving overall cooling performance. However, this thermal resistance can be eliminated by using the direct liquid cooling, where the coolant directly contact with the surface of the electronic device. Jet impingement and spray cooling are both direct liquid cooling techniques. Spray cooling was reported to have the highest heat dissipation capability owing to the direct cooling and boiling of the micron liquid droplets. However, the spray cooling contains liquid and vapor, and complicated nozzles are required, making the whole system very complicated and hard to be miniaturized. The single-phase jet impingement is not that complicated and is easy to be miniaturized, especially the confined jet impingement cooling [22–24].

Single-phase confined jet impingement cooling has been massively studied during the past decades. Jorg et al. presented an approach of direct single jet impingement liquid cooling of a typical MOSFET power module [25]. Heat transfer coefficients up to 12,000 W/m^2 K were achieved using only 10.8 cm^2 assembly space for the cooling device. The single jet impingement can only be used to cool a small heated surface because of the temperature non-uniformity. When it comes to the high power electronics with relatively large heated surface, jet array impingement must be applied. However, in the jet array impingement, the jet interference between adjacent jets prior to impingement on the surface and interaction due to collision of surface flows make the heat transfer coefficient aggressively weakened [13]. The most promising method for mitigating jet interference effects is by interlaying distributed fluid extraction ports throughout the jet array. This allows the spent fluid flows though the distributed returns to exit the impingement domain without flowing past the surrounding jets. This flow concept was introduced by Huber et al. in 1994 [26]. After this, a plenty of researches were done to study the jet array impingement with distributed extraction returns [27–32]. Bandhauer et al. developed a jet impingement direct liquid cooling solution for high performance ICs, and the average heat transfer coefficient of 13,100 W m^{-2} K^{-1} was achieved [32] but the test heat load was relatively low (less than 200 W, compared with the high power electronics).

In addition, most of the cooling methods are only focused on the cooling of one surface of the electronic device but the rest surfaces of the electronic device are not used to be cooled. As is well known, the larger heat transfer area leads to higher heat dissipation performance. For example, the size of the simulated high power chip in Fig. 1 is 10 mm × 50 mm × 4 mm. The calculated surface temperature distribution of the high power chip (2500 W) with top surface cooling and with the five-surface cooling are shown in Fig. 1(a) and (b), respectively. The only surface that is not cooled in Fig. 1(b) is used for electric

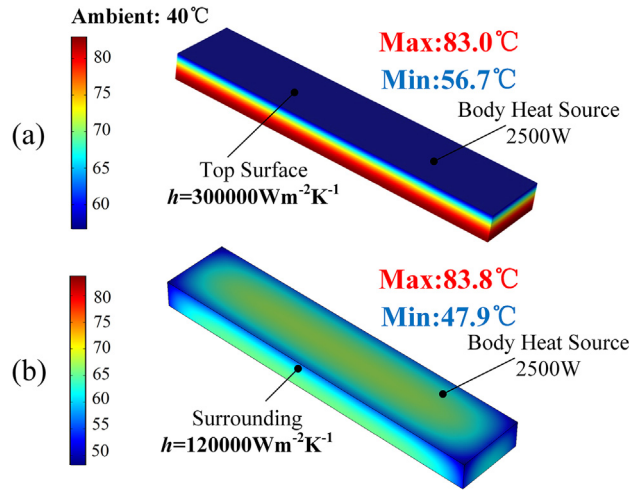

Fig. 1. Calculated surface temperature with cooling (a) only one surface and (b) 5 surfaces.

connection. To achieve the same maximum temperature, the heat transfer coefficient h of the top surface cooling only should be 2.5 times as large as that of the five-surface cooling case. The cooling surface area of the case in Fig. 1(a) is 9.8 cm^2, which is only 1.96 times (less than 2.5) as large as the cooling surface area of the case in Fig. 1(b). Therefore, the heat dissipation improvement of the body cooling in Fig. 1(b) is not only due to the increasing of the cooling surface area, but also the 3D thermal conduction of the bulk high power chip. When all the available surfaces are cooled, the thermal resistance between the coolant and the heat source is smaller than in the case that only one surface is cooled. Therefore, from this point of view, cooling all the available chip surfaces could have better cooling performance than only one surface.

Inspired by this, in this work, we developed an immersed jet array impingement cooling device (IJAICD) with distributed returns. The whole chip is immersed in the cooling device and the device provides so-called body cooling, which means high-efficient direct liquid cooling for the 5 surfaces of the high-power chip, while the rest surface of the chip is used for electric connection. Interlaying distributed extraction returns were set between impingement jets for the coolant to exit the impingement domain. The cooling device prototype was fabricated and tested by experiments. And the heat transfer process is studied by numerical simulations. The developed body cooling device may be more suitable for cooling high power and high heat flux electronics, such as the insulated gate bipolar transistor (IGBT) units, high electron mobility transistor (HEMT) units and the radar units, etc.

2. Methods

2.1. The IJAICD design and fabrication

Fig. 2(a) shows the schematic diagram of the IJAICD. The high-power chip is attached to the printed circuit board (PCB) by the TIM or solder. The contact surface is used for electric connection and the rest 5 surfaces (left surface, front surface, top surface, back surface and right surface) are cooled by impingements. The coolant flows into the IJAICD from the inlet and is then distributed to each impinging jet orifice. The coolant is directly ejected onto the corresponding heated chip surface through the orifice and is then influenced by the surface. The flow is decelerated in the axial direction and accelerated in the radial direction. The thickness of the temperature and velocity boundary layer in the impingement region is very thin and uniform due to the radial acceleration of the fluid, resulting in a very large heat transfer coefficient. As is mentioned above, the distributed return ports are set between the adjacent impinging jet orifices for the coolant to exit the impingement domain. Then the coolant flows out of the IJAICD though the outlet and carries the heat away. The IJAICD is fixed on the PCB with screws. An annular groove is machined on the device for assembling of the O-ring, which is used to prevent leaks. Fig. 2(b) shows the arrangement of the impinging jets and returns. There are five impinging walls corresponding to the five surfaces of the high-power chip. Impinging jets and returns are set on each impinging wall to provide a body cooling effect, rather than the traditional cooling for the top surface only. The heat transfer to impinging jets can be characterized by several parameters, such as the fluid Prandtl number Pr, the jet Reynolds number Re, impinging jet nozzle diameter D, nozzle-to target surface distance H and nozzle-to-nozzle spacing D_s. The geometric structure parameters of the impinging jet designed in the IJAICD in this work are shown in Fig. 2(c). The nozzle-to-target surface distance (Fig. 2(d)) between the five impinging jet walls and the five surfaces of the high-power chip are designed to be the same, namely $H = H_1 = H_2 = 0.4$ mm. There are two lines of 20 impingement nozzles on the top wall, one line of 10 nozzles on the back wall and front wall, one line of 2 nozzles on the left wall and right wall. Thus, there are totally 44 impingement nozzles with diameter 400 μm. It should be mentioned that the structure parameters of the impingement and returns were not optimized, and they were

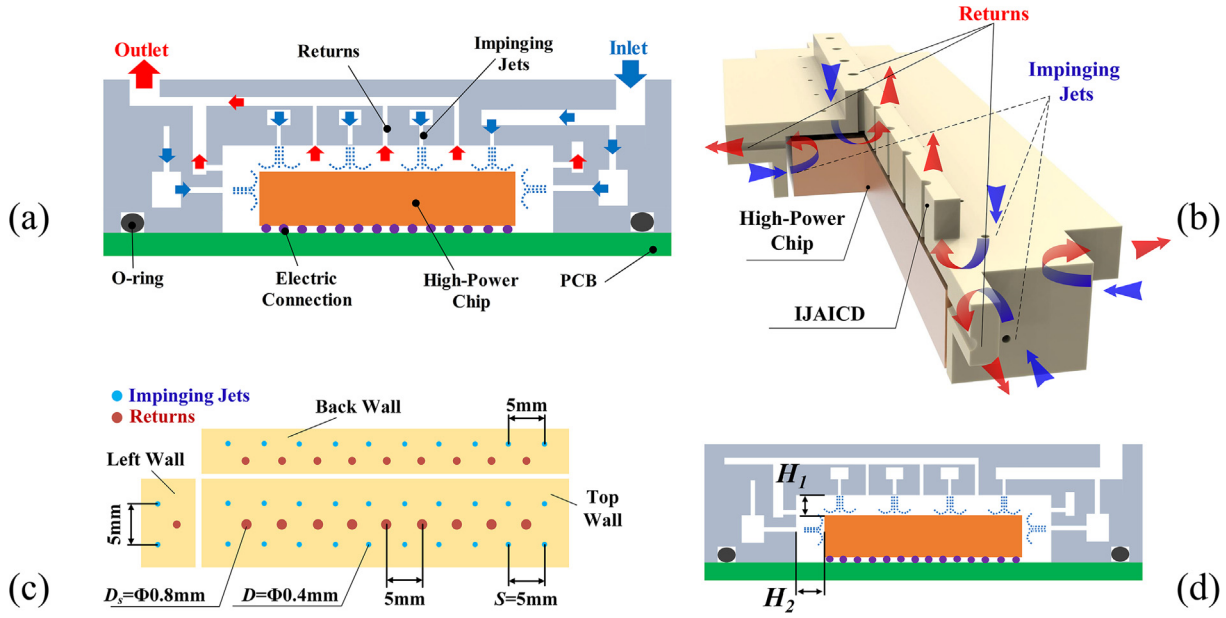

Fig. 2. Schematic diagram of (a) the structure and assembly of the IJAICD, (b) the arrangement of the impinging Jets and returns, (c) the geometric structure of the impinging jets and (d) the nozzle-to-target surface distance.

determined by referring to the previous work [27–29]. The diameter of the impingement jet orifices was determined by taking the capability and difficulty of the 3D printing process into consideration. The orifice diameter cannot be too small. Thus, we believe that the heat dissipation performance may be better if the structure parameters are optimized further.

The IJAICD was fabricated by using the Stereo lithography (SLA) 3D printing process. The advantages of the 3D printing in creating microfluidic devices were demonstrated recently [33]. The structure of the IJAICD is quite complicated due to the manifolding geometry of the jet-adjacent fluid returns and the small feature size of the whole device and the orifices of the impinging jets and returns. Traditional precision mechanical machining process can be used to fabricate the IJAICD only if the device is divided into several layers. However, the adhesion or soldering of the layers may lead to serious sealing problems, which is no a problem when using the 3D printing process. The machining precision of the 3D printing is able to reach 10–50 μm.

2.2. Experimental setup

In order to test the heat dissipation performance of the IJAICD, a test facility was constructed. Fig. 3(a) shows the schematic diagram of the test section. The IJAICD was fixed onto the PTFE plate by several screws. The O-ring was used to prevent the sealing problems. The thermal conductivity of PTFE is very low (0.24 W/m·K), making it suitable to be used as the adiabatic support plate. The structure parameters of the high-power chip in this work is 10 mm × 50 mm × 4 mm. A simulated chip made of pure copper was used to simulate the high-power chip. Seven K-type thermocouples with accuracy of ± 0.5 °C were embedded in the simulated chip to monitor and test the temperature of all the surfaces of the high-power chip (simulated chip). Seven grooves were machined for the assembly of the thermocouples as shown in Fig. 3(b). The locations of the seven thermocouples inside the simulated chip are shown in Fig. 3(c). To measure the temperature of the surface more accurately, the thermocouples should be set as close as possible to the corresponding simulated chip surface. Considering the capability of the machining process, the distances between the thermocouple and the side surface are set to be 1.3 mm, while the distances between the thermocouple and the top surface are set to be 0.15 mm (Fig. 3(c)). The TIM was coated on the thermocouple to make the thermal contact between the thermocouple and the simulated chip better. A pure copper block was fixed to the simulated chip by 16 screws to provide sufficient fastening forces. The TIM (Dow Corning TC-5121) with thermal conductivity of 3 W/m·K was coated between the simulated chip and the copper block to decrease the thermal contact resistance. Seven heating rods were inserted in the copper block to provide the heat source. Each heating rod can provide 130 W heat load in maximum. Therefore, the maximum input thermal power of the simulated chip is 910 W. A thermocouple was inserted into the bottom part of the copper block to monitor the maximum temperature of the whole system to prevent overheat of the copper block. In order to prevent the heat loss, the thermal insulation cotton was used to wrap the copper block up. The temperature of the thermal insulation cotton was measured by a thermocouple embedded in the cotton.

The test facility in this work is schematically shown in Fig. 4. The working fluid deionized water is circulated through the flow loop driven by a hydrodynamically levitated centrifugal micropump [34–36]. The maximum flow rate of the micropump is 3.5 L/min and the maximum pressure head is 160 kPa. The flow rate can be set by tuning the rotation speed of the micropump and by the valve. The volume flow rate is measured by a turbine flow meter (YF-S401) with ± 2% accuracy. The pressure drop between the outlet and inlet of the IJAICD is measured by a differential pressure gauge (HT1895) with ± 0.3% accuracy. The air-cooled heat exchanger with 16 copper pipes was used to cool the coolant and remove the heat to the ambient. A 40 μm filter was positioned upstream of the IJAICD to prevent blocking caused by impurities in the coolant. A water tank was assembled upstream of the filter and a thermocouple was put inside the water tank to measure the inlet coolant temperature. Another thermocouple was used to monitor the ambient temperature. The flow rate could be reliably controlled in the range of 300 ml/min–2.2 L/min in this test facility. The inlet temperature could be controlled at 40 °C stably by tuning the rotating speed of the fans in the air-cooled heat exchanger. DC power supplies were used to provide the input power of the heating rods, the micropump and the air-cooled heat exchanger. A data acquisition instrument was used to record the temperature data from thermocouples (see Fig. 5).

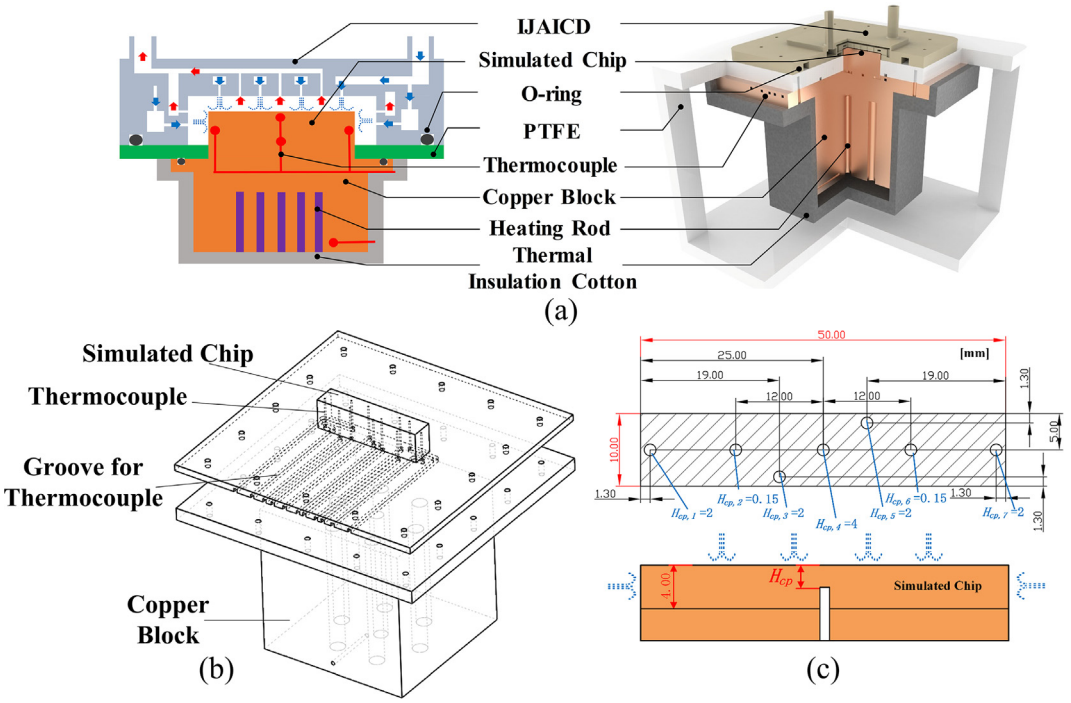

Fig. 3. (a) The schematic diagram of the test section, (b) the schematic diagram of the heated region and the assembly of the thermocouples and (c) the location of the thermocouples.

2.3. Numerical simulation

Numerical simulations were done to calculate the temperatures of the simulated chip by using the commercial multi-physics software COMSOL MULTIPHYSICS 5.3a. The CFD and Heat Transfer packages were coupled in this study to simulate the fluid flow and heat transfer process in the IJAICD. The simulated chip was set as copper and the coolant was the deionized-water. The physical property parameters of the materials used in the numerical simulation are listed in Table 1. The inlet temperature of water $T_{fluid,in}$ was set as 40 °C. The boundary heat source was added on the bottom surface of the simulated chip to meet with the boundary condition of the experiment. As is mentioned above, the heat transfers from the bottom copper block to the simulated chip, so the boundary heat source is added to the simulated chip in the experiment. To characterize the heat transfer and fluid flow process more accurately, grids were finer in the impinging jet and return regions. The grid independence test was done. The maximum temperature in the simulated chip calculated with 1,005,286, 1,432,212 and 1,891,980 grids are 86.5 °C, 86.8 °C and 84.3 °C, respectively. The discrepancies are no more than 2.88%. Considering the calculation costs, we used the case with 1,005,286 in the rest simulations, in which the 'normal' grid was selected in the COMSOL.

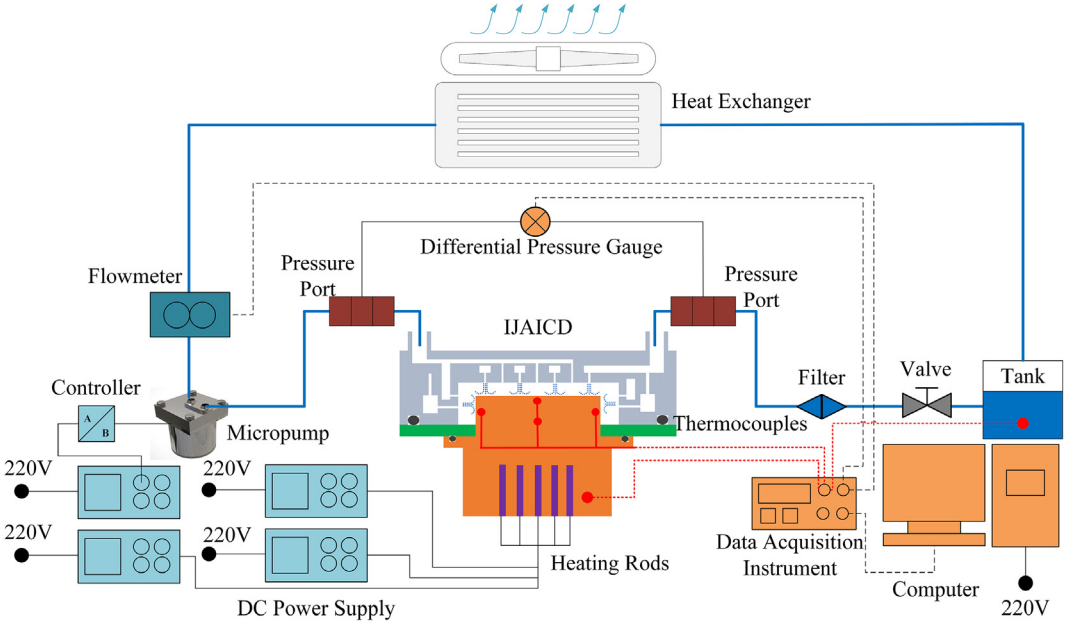

Fig. 4. The schematic diagram of the test facility.

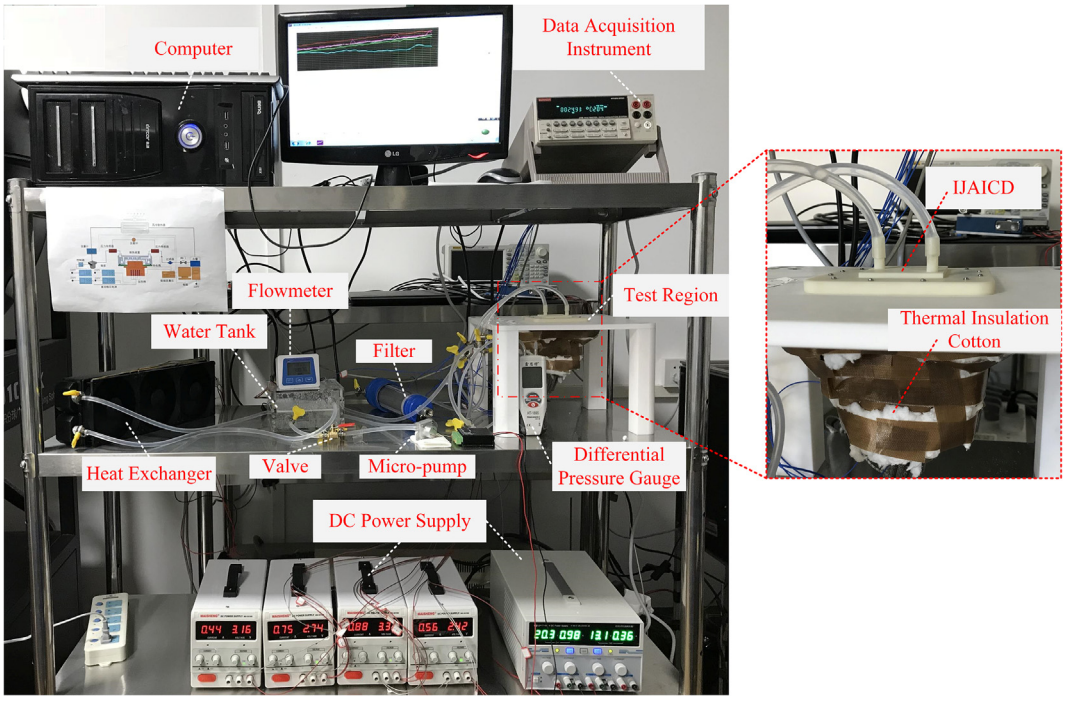

Fig. 5. Picture of the test facility.

Table 1
The physical property parameters of materials used in the numerical simulation.

Material	k (W/m·K)	ρ (kg/m^3)	μ (mPa·s)	c_p (J/Kg·K)	$T_{fluid,in}$ (°C)
Water	0.635	992.2	0.6533	4174	40
Pure copper	380	/	/	/	/

3. Results and discussion

The IJAICD was successfully fabricated by 3D printing process, as shown in Fig. 6(a)–(c). The material we used to make the IJAICD is the thermostable resin (PerForm, Somos). The dimension of the impinging jet region is 10.8 mm × 50.8 mm × 4.4 mm. Fig. 6(c) shows the view of the impinging jet and return orifices. It can be seen that the impinging jet and return orifices were machined on the top wall and other five sidewalls. The microscopic image of the impinging jet and return arrays on the top wall is shown in Fig. 6(d). The diameter of the machined impinging jet D is 424 μm, slightly larger than the designed value 400 μm. The discrepancy is due to the accuracy of the 3D printing process. The measured two jet-to-jet spacing values are 5015 μm and 4956 μm. The diameter of the extraction return orifice D_s is 822 μm.

The range of the test flow rate is from 500 ml/min to 2100 ml/min in experiments and numerical simulations. The range of the input heat power if from 100 W to 800 W. The numerically calculated temperature distribution of top, front and right of the simulated chip is shown in Fig. 7. Results indicate that the minimum temperature regions are at the corners of the simulated chip. This phenomenon is similar with the case in Fig. 1(b). It is believed to be benefit from the body cooling effect and the 3D thermal conduction in the simulated chip. In Fig. 7, the impingement patterns and the extraction return patterns can be observed obviously through the temperature distribution of the surfaces. The temperature of the impingement domain is much lower and the the temperature of the extraction return domain is much higher than the surrounding domain. The highest temperature theoretically exists at the center of the bottom surface, so the bottom of the front surface has the highest temperature in Fig. 7. When the flow rate increases from 1500 ml/min to 2000 ml/min, the jet Reynolds number and the jet velocity are both increased, resulting in larger heat transfer coefficient. As the IJAICD provides body cooling for all the five surfaces, the temperature at any position decreases simultaneously.

The numerically calculated surface temperature on line A, line B and line C (Fig. 7) are shown in Fig. 8(a). The temperature variation trends of line A on the top surface and line B on the front surface are the same, owing to the same arrangement of impinging jets. The macroscopic trends for temperature of line A, B, and C are firstly increased and then decreased. There are 10 valleys for line A and B, 2 valleys for line C with lower temperature, indicating the existence of 10 impinging jets on line A and B and 2 impinging jets on line C. The calculated local heat transfer coefficients are shown in Fig. 8(b). The local heat transfer coefficient is calculated as

$$h_{loc} = \frac{q_{loc}}{(T_{loc} - T_{fluid,in})} \quad (1)$$

where q_{loc} is the local heat flux normal to the surface and T_{loc} is the local surface temperature. The heat transfer coefficients of line A, B and C show great coincidence. The heat transfer coefficient at the stagnation point of the impinging jets could reach as high as 2.6 × 10^5 W/m^2·K but that of the rest places decrease heavily to be lower than 10^4 W/m^2·K. It can be seen that the maximum local heat transfer coefficients of different jets for the same surface have some differences. We believe that this phenomenon is mainly due to the flow maldistribution. The average heat transfer coefficients for the surface are also depended on the area ratio the impingement jets to the surfaces. According to the structure design, the area ratio of the impingement jets to the surfaces are almost the same, indicating that the impingement jets for the top, front and right surfaces have almost the same cooling performance. In Fig. 8(b), it can be seen that the local heat transfer coefficients at the edge of the surfaces are very large. The local heat flux normal to the surface at the edges may be very large, due to the influence from the adjacent surfaces. Therefore, the calculated h_{loc} at the edges are large based on Eq. (1). This helps to explain the reason why the temperatures at corners of the simulated chip are relatively low. It is a combined effect of the body cooling and the 3D thermal conduction of the simulated chip.

It also can be observed that the temperature on the right surface

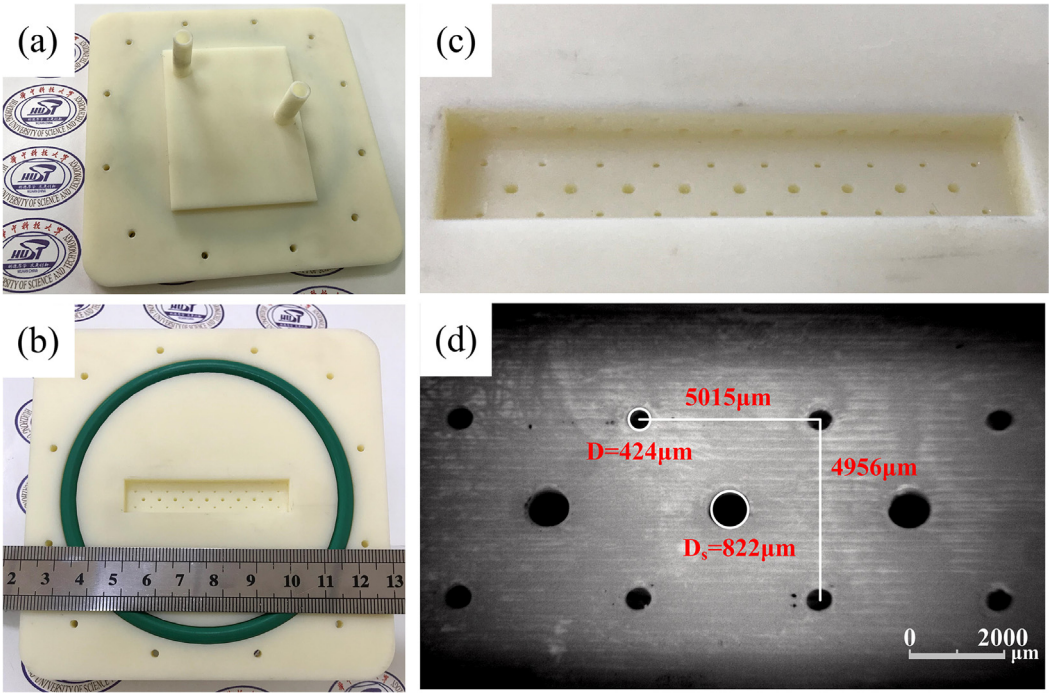

Fig. 6. (a) Top view of the fabricated IJAICD prototype, (b) bottom view of the fabricated IJAICD prototype, (c) view of the impinging jet and return orifices and (d) the microscopic image of the impinging jet and return arrays on the top wall.

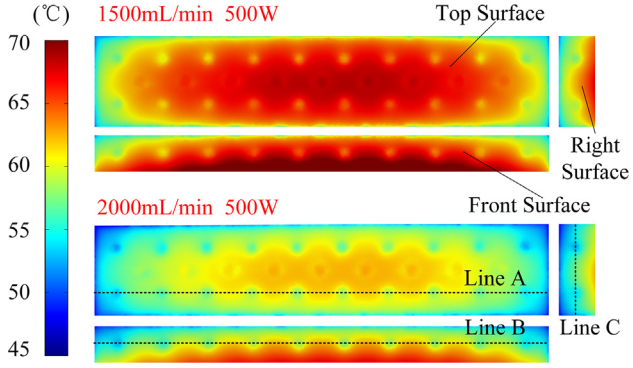

Fig. 7. Numerically calculated temperature distribution on top, right and front surface of the simulated chip.

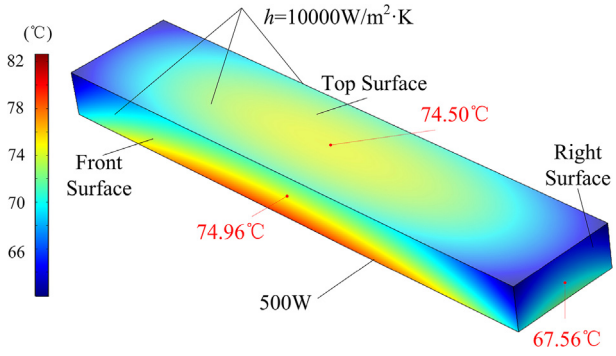

Fig. 9. Numerical simulation of the simulated chip with boundary heat source 500 W and homogeneous heat transfer coefficient h = 10,000 W/m^2·K.

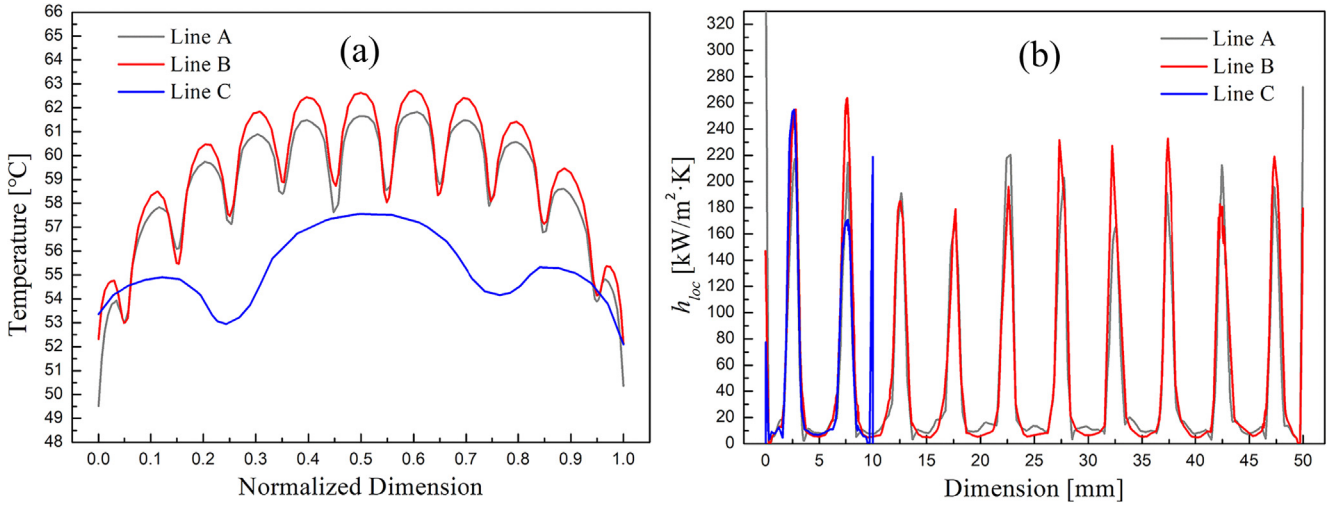

Fig. 8. Numerical calculation for (a) the surface temperature on line A, B and C with volume flow rate 2000 ml/min and input heat power 500 W and (b) the local heat transfer coefficient on line A, B and C with volume flow rate 2000 ml/min and input heat power 500 W.

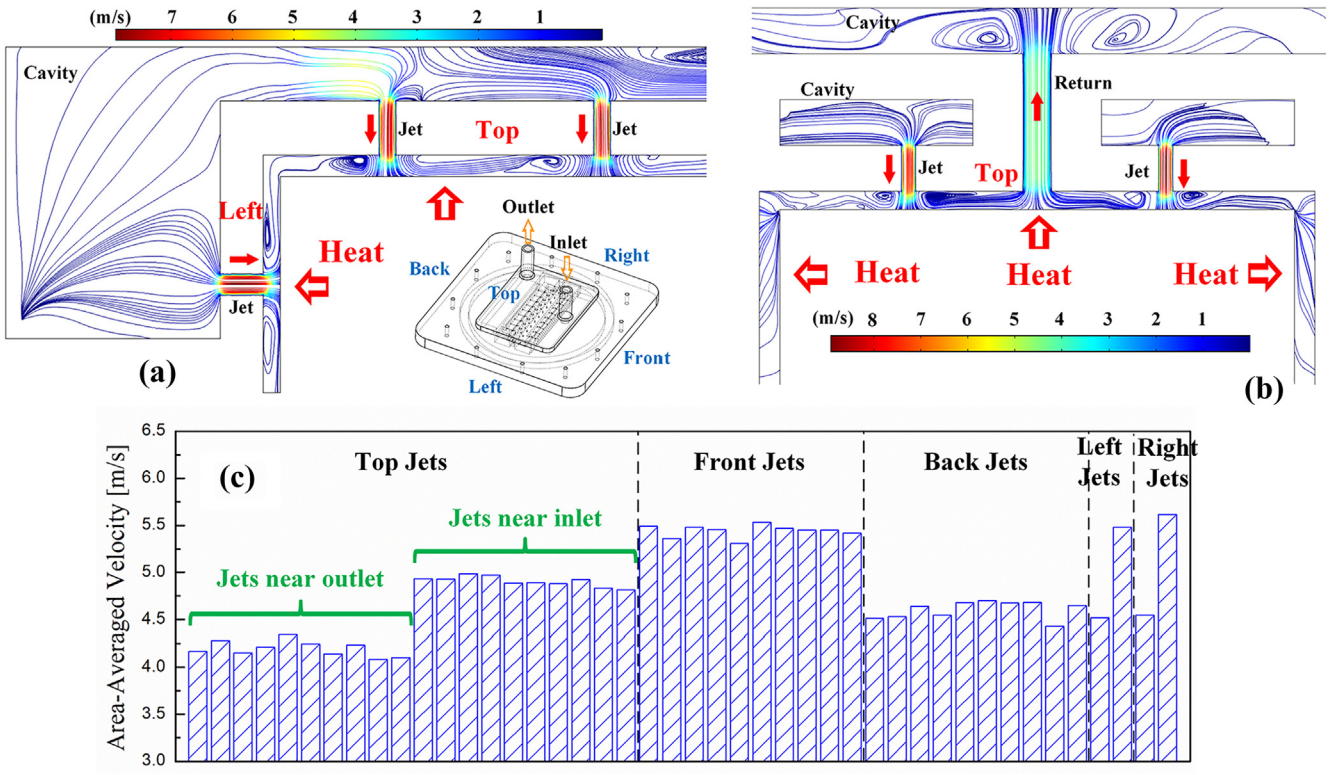

Fig. 10. Simulation results with 2000 ml/min flow rate and 500 W input heat power of (a) streamline of the jets and (b) streamline of the jets and returns and (c) the area-averaged flow velocity of the 44 jet nozzles.

(line C) is much lower than that on the top and front surfaces (line A and line B). As is explained before, the impinging jets provide equal heat transfer coefficients and equal cooling performance to the five surfaces. Thus, the only explanation is that the heat fluxes are different on these surfaces. This phenomenon also exists in the case shown in Fig. 9. We simulated the 3D thermal conduction in the simulated chip by adding equal heat transfer coefficients on the five surfaces and adding the boundary heat source on the bottom surface. Results show that the right surface has the lowest temperature. This explains that the temperature difference and heat flux difference are mainly due to the combined effect of the body cooling effect and 3D thermal conduction. Body cooling makes the coolant more closely to the heat source, and the thermal conducive resistance from heat source to the surface is non-uniform, due to the 3D thermal conduction of the bulk simulated chip. This is also why the required heat transfer coefficient ratio of the one surface cooling to the body cooling is much larger than the heat transfer area ratio of the body cooling to the one surface cooling (Fig. 1).

The simulation results of the streamline of jets and returns and the flow distribution of jets are shown in Fig. 10. The simulation was conducted under the 2000 ml/min flow rate and 500 W input heat power. Due to the small cross-section area, the flow velocity of the jet is quite large (up to 9.08 m/s). So that the extremely thin boundary layer is formed on the chip surface, resulting in large heat transfer coefficient. It can be obtained in Fig. 10(a) that there is no obvious flow interaction between the top jets and between the top jets and the left jets. This is mainly because of the existence of the returns (Fig. 10(b)). Despite of the existence of the relatively large cavity, which acts as the buffer before the fluid flows into jets, the flow maldistribution still exists. This is mainly due to the pressure difference and the flow resistance between the inlet and outlet. The cross-section area-averaged flow velocity of all the 44 jets are shown in Fig. 10(c). The flow maldistribution can be clearly observed on the 2×10 top jets. 10 jets near the inlet have larger flow velocity and the 10 jets near the outlet have smaller flow velocity. The slight flow maldistribution effect exists even between the 10 jets of the same row. The same phenomenon can be found in the front, back, left and right jets. The flow maldistribution effect may lead to slightly different convective heat transfer coefficients of jets (Fig. 8(b)).

The experimental tested temperatures are shown in Fig. 11. The tested average temperature and maximum temperature of the simulated chip are in great agreement with simulated results. The maximum temperature was represented by temperature measured by thermocouple number 4. The average temperature was calculated as

$$T_{ave} = \frac{1}{7}\sum_{j=1}^{7} T_j \tag{2}$$

where T_j (j = 1, 2, …, 7) represents the temperature measured by the jth thermocouple. The temperature changes linearly with increasing the input thermal power. The measured average temperature with input heat power 550 W and flow rate 1000 ml/min is only 77.0 °C, where the effective heat flux is 110 W/cm^2. The temperature rise is only 37 °C, based on the inlet fluid temperature of 40 °C. From Fig. 10(c), it can be observed that the maximum input heat power reaches 800 W. With the flow rate of 2000 ml/min, the average temperature of the simulated chip at the input heat power of 800 W is only 78.7 °C, where the effective heat flux is 160 W/cm^2. Even the maximum temperature in the simulated chip is only 86.8 °C, which is a very safe and comfort temperature for high-power electronics.

Results of the tested copper block temperature and the temperature of the thermal insulation cotton are shown in Fig. 11(d). The results were tested with the flow rate of 2000 ml/min. The temperatures increase linearly with increasing the input heat power. The maximum temperature of the cotton is 65.3 °C. The heat loss usually increases with increasing the heating power. Therefore, we calculated the maximum heat loss of the test section at the input heat power of 800 W. The heat loss was briefly calculated using the Newton's law of cooling $q_{loss} = h_n \times A_c \times (T_c - T_a)$, where h_n is the natural convective heat transfer coefficient, A_c is the surface area of the copper block, T_c is the

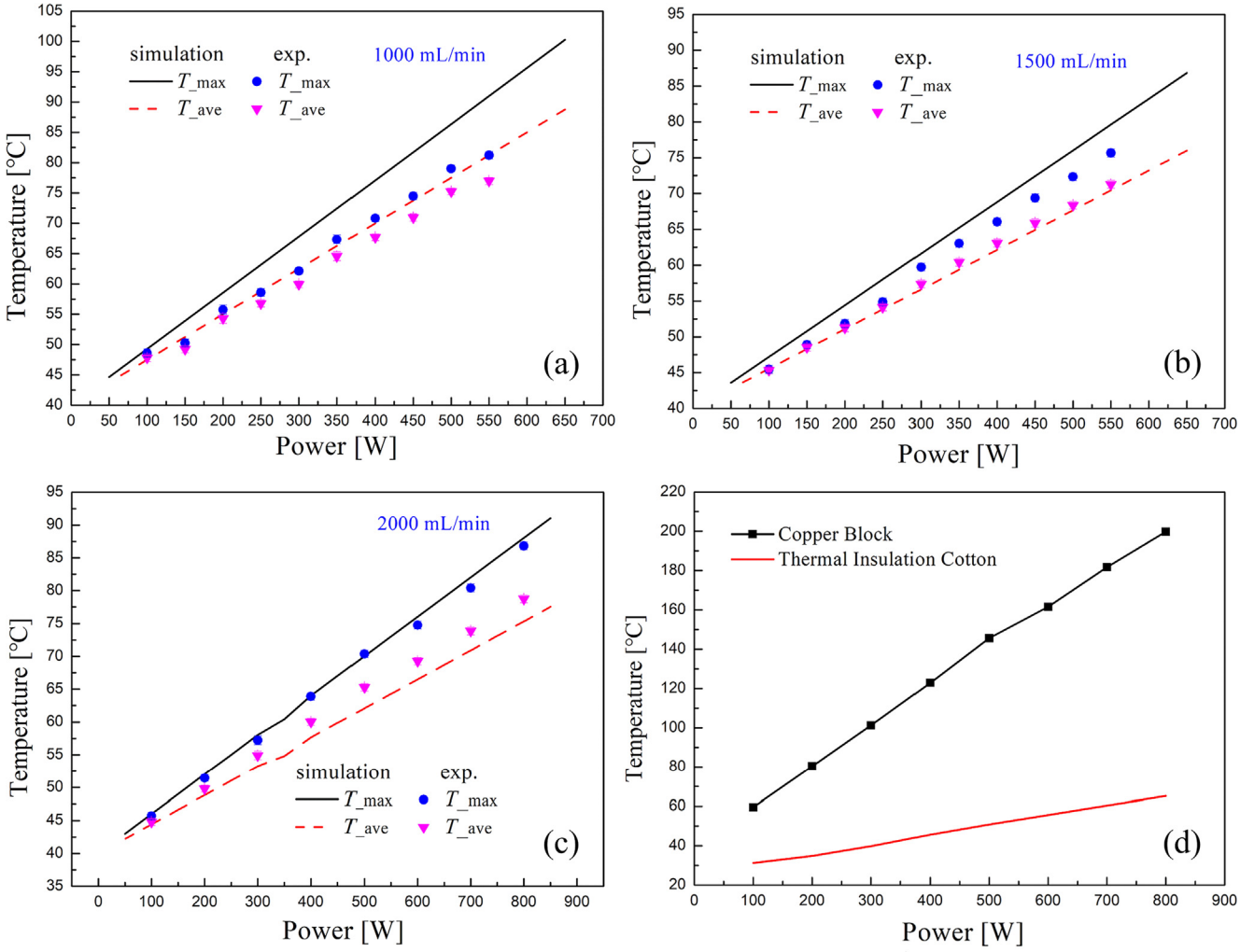

Fig. 11. (a) Tested temperature varies with input thermal power at flow rate of 1000 ml/min, (b) tested temperature varies with input thermal power at flow rate of 1500 ml/min, (c) tested temperature varies with input thermal power at flow rate of 2000 ml/min, and (d) the tested temperature of copper block and thermal insulation cotton.

cotton temperature and T_a is the ambient temperature. h_n is set to be 10 W/m^2·K, which is believed to be almost the maximum natural convective heat transfer coefficient in reality. The A_c was calculated to be 368.8 cm^2. The ambient temperature is 22 °C in minimum. Therefore, the calculated q_{loss} should be 15.97 W, which is only 2% of the input heat power (800 W). It means that the heat loss in this work should be no more than 2%.

Fig. 12(a) shows that the temperature of the simulated chip decreases with increasing the volume flow rate. When the input heat power is 500 W, the maximum chip temperature is 68.2 °C with the volume flow rate of 2100 ml/min. And, the maximum chip temperature is only 57.2 °C with the same volume flow rate, when the input heat power is 300 W. It can be observed from the trend of the results that when the volume flow rate is further increased, the temperature should be even lower. This indicates that the fluid convection thermal resistance is the main thermal obstacle even if the volume flow rate is very large. There are two reasons to explain it. One is that, as for the IJAICD, the convection thermal resistance is the only thermal resistance between the coolant and the chip, because of the direct liquid cooling. The other is that, as for the impinging jet liquid cooling, the heat transfer coefficient always increase with the volume flow rate and will not converge to a value, due to the better heat transfer performance when the jet velocity is larger. The pressure drop of the IJAICD as a function of volume flow rate is shown in Fig. 12(b). The pressure drop increases with the volume flow rate. The pressure drop is 19.8 kPa as the volume flow rate reaches 2000 ml/min, which is a very small pressure drop. As a comparison, the pressure drop of the microchannel heat sink developed by Sharma *et al.* [37] reaches 40 kPa when the volume flow rate is only 1200 ml/min.

Fig. 13 shows the total thermal resistance as a function of volume flow rate. The total thermal resistance is calculated as $R_{tot} = (T_{ave} - T_{fluid,in})/P_{heat}$, where P_{heat} is the input heat power. The total thermal resistance decreases heavily with increasing the volume flow rate. The minimum total thermal resistance of 0.05 K/W was realized when the volume flow rate is 2100 ml/min. Assuming that the thermal conductivity of the TIM is 3 W/m·K, and considering the thickness of 50 μm, the thermal resistance of the TIM used on the surface of the simulated chip should be 0.033 K/W. Therefore, the total thermal resistance of the IJAICD is able to be compared with the thermal conductive resistance of the TIM, which is only a small part of the whole traditional heat sink.

We calculated the effective wall heat transfer coefficient h_{eff_wall} and the foot print heat transfer coefficient h_{fp} and the results are shown in Fig. 14(a). They are calculated as

$$h_{eff\_wall} = \frac{q}{(A_{top} + A_{left} + A_{front} + A_{right} + A_{back})(T_{wall} - T_{fluid,in})} \quad (3)$$

where A represents the surface area and T_{wall} is the averaged wall

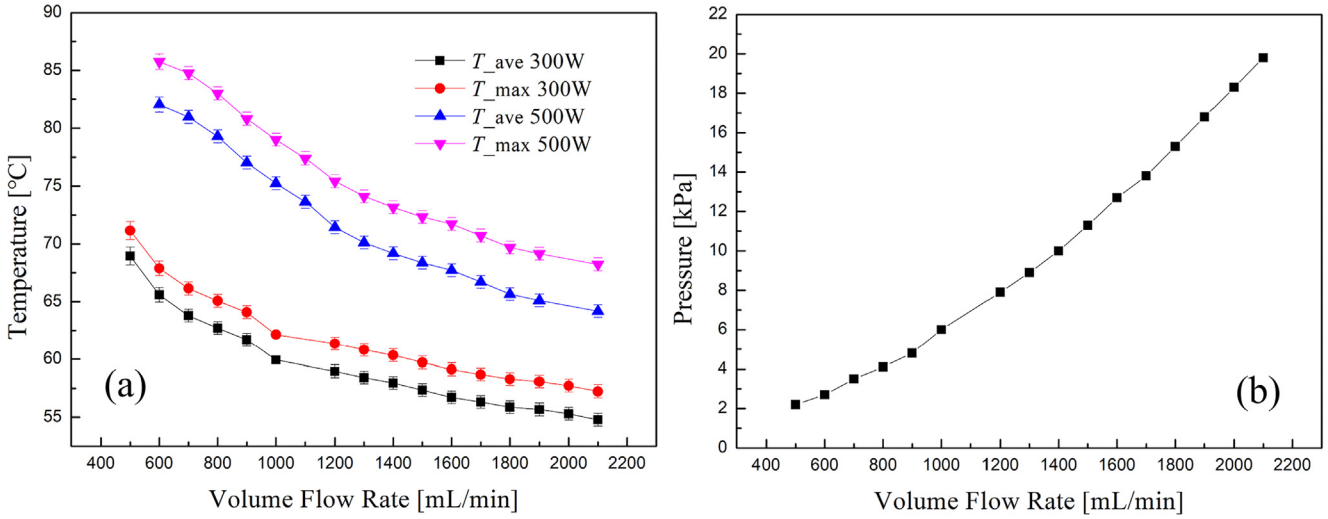

Fig. 12. (a) The average and maximum temperature of the simulated chip as a function of the volume flow rate and (b) The pressure drop of the IJAICD as a function of the volume flow rate.

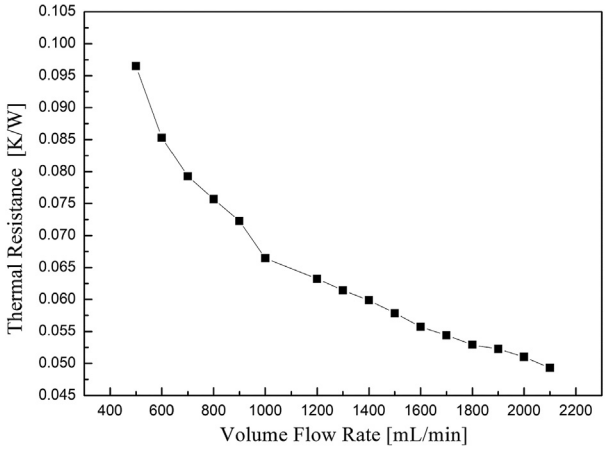

Fig. 13. The total thermal resistance as a function of volume flow rate.

temperature that is given by

$$T_{wall} = \frac{T_1 + T_2 + T_3 + T_5 + T_6 + T_7}{6} \tag{4}$$

h_{fp} represents the effective heat transfer coefficient that calculated as the traditional one-surface cooling situation, and is given by

$$h_{fp} = \frac{q}{A_{top}(T_{ave} - T_{fluid.in})} \tag{5}$$

The heat transfer coefficients increase with the volume flow rate. The input heat power has nearly no effect on the heat transfer coefficients. The maximum h_{fp} in this work can reach 41,377 W/m^2·K with the volume flow rate of 2100 ml/min. The effective wall Nusselt number Nu_{eff_wall} and the foot print Nusselt number Nu_{fp} as a function of Re are shown in Fig. 14(b). The Nusselt number and the Re were calculated based on the jet diameter. We did the non-linear fitting of these two parameters, and the fitting results are

$$Nu_{eff\_wall} = 0.32 \times Re^{0.453} \tag{6}$$

and

$$Nu_{fp} = 0.685 \times Re^{0.4376} \tag{7}$$

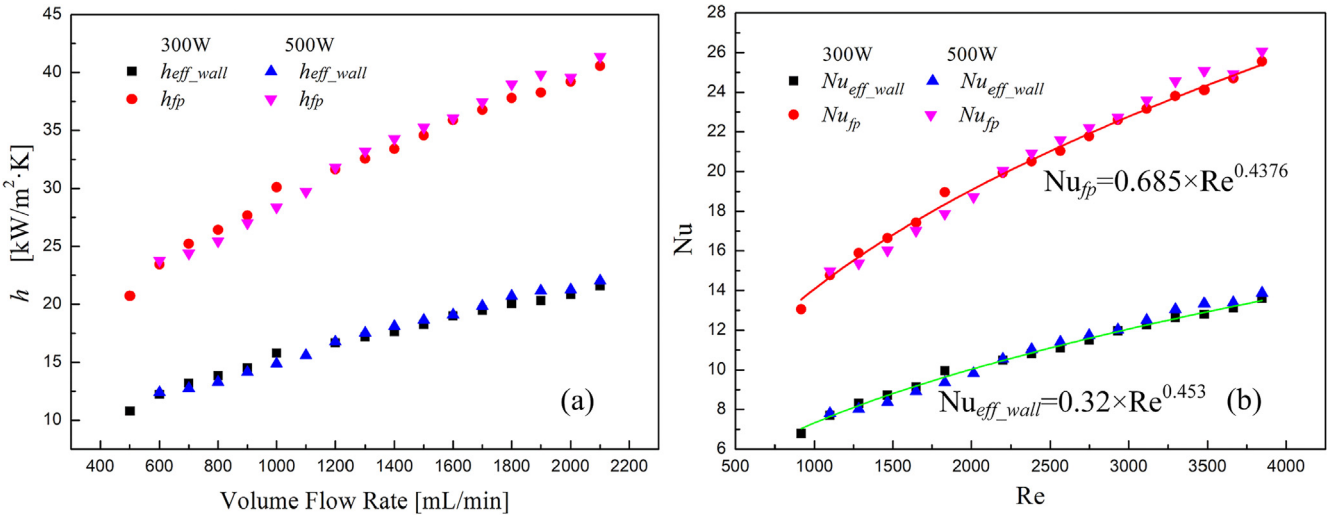

Fig. 14. (a) The effective wall heat transfer coefficient h_{eff_wall} and the foot print heat transfer coefficient h_{fp} as a function of the volume flow rate and (b) Nu_{eff_wall} and Nu_{fp} as a function of Re.

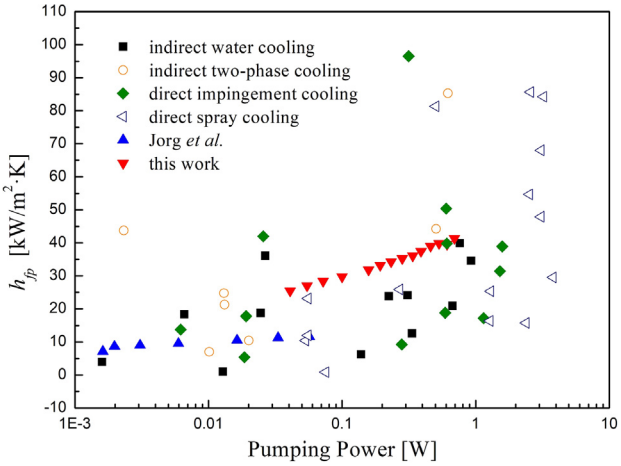

Fig. 15. Comparison of the h_{fp} of the IJAICD as a function of pumping power with other liquid cooling studies.

The calculated h_{fp} in this work is compared with other liquid cooling studies, and the results are shown in Fig. 14. The data of other liquid cooling studies are obtained from the previous review [38]. Results show that the IJAICD has good cooling performance and relatively large heat transfer coefficient. It is promising for cooling the high power electronic devices (see Fig. 15).

4. Conclusions

In this work, we developed an immersed jet array impingement cooling device with distributed returns. The IJAICD provides high efficient body cooling to the high-power chip. Five surfaces of the chip are directly liquid cooled by impinging jets. We fabricated the prototype of the IJAICD and established a test facility to test the heat dissipation performance of the IJAICD. Numerical simulations were done to study the heat transfer process of the IJAICD. The test input heat power for the simulated chip is as high as 800 W to simulate the high-power chips. The low temperature regions exist at the corners of the simulated chip, due to the combine effect of the body cooling and the 3D thermal conduction. Results show that the temperature of the simulated chip increases linearly with increasing the input heat power. The measured average temperature with input heat power 550 W and flow rate 1000 ml/min is only 77.0 °C. The temperature rise is only 37 °C with the inlet fluid temperature of 40 °C. The average temperature of the simulated chip at the input heat power of 800 W is only 78.7 °C with the flow rate reaches 2000 ml/min. According to the measured temperature of the thermal insulation cotton, the heat loss of the test section is calculated to be no more than 2% of the whole input heat power. The minimum total thermal resistance of the IJAICD reaches 0.05 K/W with the volume flow rate 2100 ml/min. The body cooling device (IJAICD) is able to take full advantage of the heat dissipation area of the high-power chip than traditional one-surface cooling methods. And the 3D thermal conduction of the high-power chip can be take advantage of in the body cooling method. Therefore, the IJAICD may be a promising option for cooling the high-power electronic devices.

Acknowledgements

The authors would like to acknowledge the financial support by National Natural Science Foundation of China (51625601, 51576078, 51606074), the Ministry of Science and Technology of the People's Republic of China (Project No. 2017YFE0100600), the Financial support from Creative Research Groups Funding of Hubei Province (2018CFA001).

Appendix A. Supplementary material

Supplementary data to this article can be found online at https://doi.org/10.1016/j.applthermaleng.2019.114259.

References

[1] C. Qian, A.M. Gheitaghy, J. Fan, H. Tang, B. Sun, H. Ye, G. Zhang, Thermal management on IGBT power electronic devices and modules, IEEE Access 6 (2018) 12868–12884.
[2] X.B. Luo, R. Hu, S. Liu, K. Wang, Heat and fluid flow in high-power LED packaging and applications, Prog. Energ. Combust. Sci. 56 (2016) 1–32.
[3] R.C. Chu, R.E. Simons, M.J. Ellsworth, R.R. Schmidts, V. Cozzolino, Review of cooling technologies for computer products, IEEE Trans. Dev. Mater. Res. 4 (4) (2004) 568–585.
[4] S.M. SOhel Murshed, C.A. Nieto de Castro, A critical review of traditional and emerging techniques and fluids for electronics cooling, Renew. Sust. Energy Rev. 78 (2017) 821–833.
[5] E. Laloya, O. Lucia, H. Sarnago, J.M. Burdio, Heat management in power converters: from state of the art to future ultrahigh efficiency systems, IEEE Trans. Power Electr. 31 (11) (2016) 7896–7908.
[6] R. Hu, S. Zhou, Y. Li, D. Lei, X. Luo, C. Qiu, Illusion thermotics, Adv. Mater. 30 (2018) 1707237.
[7] Y. Ma, W. Lan, B. Xie, R. Hu, X. Luo, An optical-thermal model for laser-excited remote phosphor with thermal quenching, Int. J. Heat Mass Trans. 116 (2018) 694–702.
[8] R. Schmidt, Challenges in electronic cooling-opportunities for enhanced thermal management techniques-microprocessor liquid cooled minichannel heat sink, Heat Transfer Eng. 25 (3) (2004) 3–12.
[9] B. Xie, H. Liu, R. Hu, C. Wang, J. Hao, K. Wang, X. Luo, Targeting cooling for quantum dots in white QDs-LEDs by hexagonal boron nitride platelets with electrostatic bonding, Adv. Funct. Mater. 28 (2018) 1801407.
[10] S. Yang, D. Xiang, A. Bryant, P. Mawby, L. Ran, P. Tavner, Condition monitoring for device reliability in power electronic converters: a review, IEEE Trans. Power Electr. 25 (11) (2010) 2734–2752.
[11] J.R. Black, Electromigration – a brief survey and some recent results, IEEE Trans. Electron Dev. (1969) 338–347.
[12] S.T. Kadam, R. Kumar, Twenty first century cooling solution: Microchannel heat sinks, Int. J. Therm. Sci. 85 (2014) 73–92.
[13] B. Weigand, S. Spring, Multiple jet impingement – a review, Heat Transf. Res. 42 (2) (2011) 101–142.
[14] C.F. Ma, Y.P. Gan, Y.C. Tian, D.H. Lei, T. Gomi, Liquid jet impingement heat transfer with or without boiling, J. Therm. Sci. 2 (1) (1993) 32–49.
[15] J.A. Fitzgerald, S.V. Garimella, A study of the flow field of a confined and submerged impinging jet, Int. J. Heat Mass Trans. 41 (8–9) (1998) 1025–1034.
[16] G. Liang, I. Mudawar, Review of spray cooling – Part 1: Single-phase and nucleate boiling regimes, and critical heat flux, Int. J. Heat Mass Trans. 115 (2017) 1174–1205.
[17] W. Wu, H. Bostanci, L.C. Chow, S.J. Ding, Y. Hong, M. Su, J.P. Kizito, L. Gschwender, C.E. Snyder, Jet impingement and spray cooling using slurry of nanoencapsulated phase change materials, Int. J. Heat Mass Trans. 54 (2011) 2715–2723.
[18] C.S. Sharma, M.K. Tiwari, S. Zimmermann, T. Brunschwiler, G. Schlotting, B. Michel, D. Poulikakos, Energy efficient hotspot-targeted embedded liquid cooling of electronics, Appl. Energy 138 (2015) 414–422.
[19] B. Sun, H. Liu, Flow and heat transfer characteristics of nanofluids in a liquid-cooled CPU heat radiator, Appl. Therm. Eng. 115 (2017) 435–443.
[20] R. Wu, X. Zhang, Y. Fan, R. Hu, X. Luo, A bi-layer compact thermal model for uniform chip temperature control with non-uniform heat sources by genetic-algorithm optimized microchannel cooling, Int. J. Therm. Sci. 136 (2019) 337–346.
[21] T. Brunschwiler, H. Rothuizen, M. Fabbri, U. Kloter, B. Michel, Direct jet-impingement cooling with micron-sized nozzle array and distributed return architecture, in: Proc. Inter-soc. Conf. Thermomech. Phenom. Electron. Syst., 2006, pp. 693-699.
[22] C.T. Chang, G. Kojasoy, F. Landis, Confined single- and multiple-jet impingement heat transfer I. Turbulent submerged liquid jets, Int. J. Heat Mass Trans. 38 (5) (1995) 833–842.
[23] C.-Y. Li, S.V. Garimella, Prandtl-number effects and generalized correlations for confined and submerged jet impingement, Int. J. Heat Mass Trans. 44 (2001) 3471–3480.
[24] C.Y. Zhang, T. Wang, D.H. Chen, F.J. Hong, P. Cheng, Confined jet array impingement cooling with spent flow distraction using NEPCM slurry, Int. Commun. Heat Mass 77 (2016) 140–147.
[25] J. Jorg, S. Taraborrelli, G. Sarriegui, R.W.D. Doncker, R. Kneer, W. Rohlfs, Direct single impinging jet cooling of a MOSFET power electronic module, IEEE T. Power Electr. 33 (5) (2018) 4224–4237.
[26] A.M. Huber, R. Viskanta, Effect of jet-jet spacing on convective heat transfer to confined impinging arrays of axisymmetric air jets, Int. J. Heat Mass Trans. 37 (18) (1994) 2859–2869.
[27] G. Natarajan, R.J. Bezama, Microjet cooler with distributed returns, Heat Transf. Eng. 28 (8–9) (2007) 779–787.
[28] A.S. Rattner, General characterization of jet impingement array heat sinks with interspersed fluid extraction ports for uniform high-flux cooling, J. Heat Transfer 139 (8) (2017) 82201–82211.

[29] T. Brunschwiler, H. Rothuizen, M. Fabbri, U. Kloter, B. Michel, R.J. Bezama, G. Natarajan, Ieee, direct liquid jet-impingement cooling with micronsized nozzle array and distributed return architecture, in: Proc. 10th Intersoc. Conf. Therm. Thermomechanical Phenom. Electron. Syst. vol. 1, no. 2, 2006, pp. 196–203.
[30] Y. Han, B.L. Lau, H. Zhang, X. Zhang, Package-level si-based micro-jet impingement cooling solution with multiple drainage micro-trenches, in: Proc. 16th Electron. Packag. Technol. Conf. EPTC, 2014, pp. 330–334.
[31] A. Husain, N.A. Al-Azri, N.Z.H. Al-Rawahi, A. Samad, Comparative performance analysis of microjet impingement cooling models with different spent-flow schemes, J. Thermophys. Heat Transf. 30 (2) (2016) 466–472.
[32] T.M. Bandhauer, D.R. Hobby, C. Jacobsen, D. Sherrer, Thermal performance of micro-jet impingement device with parallel flow, jet-adjacent fluid removal, Proceedings of the ASME 2018 16th International Conference on Nanochannels, Microchannels, and Minichannels, (2018).
[33] A.K. Au, N. Bhattacharjee, L.F. Horowitz, T.C. Chang, A. Folch, 3D-printed microfluidic automation, Lab. Chip 15 (8) (2015) 1934–1941.
[34] R. Wu, B. Duan, F. Liu, H. Wu, Y. Cheng, X. Luo, Design of a hydro-dynamically levitated centrifugal micro-pump for the active liquid cooling system, Electronic Packaging Technology (ICEPT), 18th International Conference on, IEEE, 2017, pp. 402–406.
[35] X. Luo, F. Liu, B. Duan, H. Wu, J. Hu, X. Yu, A hydrodynamic levitated mechanical micropump, Chinese Patent, ZL 2016.1.1139270.6.
[36] X. Luo, R. Wu, B. Duan, F. Liu, A hydrodynamic levitated mechanical pump with grooved bearings, Chinese Patent, ZL 201710339001.2.
[37] C.S. Sharma, G. Schlottig, T. Brunschwiler, M.K. Tiwari, B. Michel, D. Poulikakos, A novel method of energy efficient hotspot-targeted embedded liquid cooling for electronics: an experimental study, Int. J. Heat Mass Trans. 88 (2015) 684–694.
[38] A.C. Kheirabadi, D. Groulx, Cooling of server electronics: A design review of existing technology, Appl. Therm. Eng. 105 (2016) 622–638.